Coastal Engineering 179 (2023) 104242

Contents lists available at ScienceDirect

Coastal Engineering

journal homepage: www.elsevier.com/locate/coastaleng

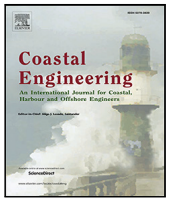

An empirical model for velocity in rough turbulent oscillatory boundary layers

Danny Dunbar [a], Dominic A. van der A [a,*], Tom O'Donoghue [a], Pietro Scandura [b]

[a] School of Engineering, University of Aberdeen, King's College, Aberdeen, AB24 3UE, Scotland
[b] Department of Civil Engineering and Architecture, University of Catania, Via Santa Sofia, 64 95123, Catania, Italy

ARTICLE INFO

Keywords:
Oscillatory flow
Boundary layers
Rough turbulent flow
Empirical model

ABSTRACT

A novel empirical model for the streamwise velocity in oscillatory boundary layer flow, valid in the rough turbulent regime, is presented. The model consists of simple expressions that require only the free-stream velocity time-series and equivalent sand-grain roughness length of the bed to be known *a priori*. A frequency-independent attenuation and phase lead is assumed for all flow harmonics, expressions for which are extracted from data from previous experimental studies made in 3 different oscillatory flow tunnels. Only the oscillating component of the flow is considered in the model; steady streaming is neglected. Errors in kinematics predicted by the model are typically two orders of magnitude smaller than the maximum oscillatory velocity in the free-stream. Hence, it is well-suited to engineering application due to its simplicity and accuracy.

1. Introduction

Over the past few decades, considerable research effort has been directed toward the study of oscillatory boundary layer flows similar to those that occur at the seabed under sea waves in the coastal zone. Using dimensional analysis, Jonsson (1966) demonstrated that the boundary layer thickness δ_{bl} and friction factor f_w are functions of the Reynolds number $Re = UA/\nu$ and inverse relative roughness A/k_s, where U is the maximum oscillatory velocity in the free-stream, $A = U/\omega$ is the orbital semi-excursion, $\omega = 2\pi/T$ is the flow angular frequency, T is the flow period, ν is the fluid kinematic viscosity and k_s is the equivalent sand-grain roughness length (Nikuradse, 1933). Several laboratory studies have been previously conducted to investigate oscillatory boundary layer hydrodynamics; key studies are indicated in the Re–A/k_s regime diagram shown in Fig. 1. Most early experiments involved sinusoidal oscillatory flows. In the natural coastal environment, this assumption is simplistic because waves, and hence, the free-stream velocity time-series near the seabed, develop significant skewness and asymmetry as a result of shoaling processes (e.g. Malarkey and Davies, 2012). Many studies (e.g. King, 1991; Dibajnia and Watanabe, 1998; van der A et al., 2010; Silva et al., 2011) have demonstrated the importance of flow skewness and asymmetry for the transport of sediments. These sediment transport studies have been complemented by more recent research in which the effects of skewness and asymmetry on rough-wall boundary layer hydrodynamics have been experimentally investigated in oscillatory flow tunnel (OFT) facilities (van der A et al., 2011; Yuan and Madsen, 2014; O'Donoghue et al., 2021; Dunbar, 2022). An OFT is a U-tube facility in which a piston is used to generate an oscillatory flow. OFT facilities are well suited to the study of flows analogous to those that occur under real waves due to the capacity of a relatively small facility to generate large amplitude oscillatory flows. Additionally, the amplitude and phase of each harmonic component of the flow in an OFT can be precisely controlled. However, unlike the flow under surface gravity waves, the mean flow field in an OFT is horizontally uniform and lacks a vertical component. Xie et al. (2021) conducted a study of flows with Re and A/k_s values similar to van der A et al. (2011), Yuan and Madsen (2014), O'Donoghue et al. (2021) and Dunbar (2022) in a large wave flume. In this type of facility, the flow is naturally comprised of multiple harmonics but their relative amplitude and phase cannot be controlled.

The studies of van der A et al. (2011), Yuan and Madsen (2014), O'Donoghue et al. (2021), Xie et al. (2021) and Dunbar (2022) primarily cover the rough turbulent regime (see Fig. 1). This regime has been a particular focus for recent study because it represents the bottom boundary layer under storm-generated waves over a seabed comprised of sand or gravel, which is an especially important scenario for the transport of sediments.

Several authors have used a variety of numerical approaches ranging from Reynolds-averaged Navier–Stokes (RANS) models with $k-\varepsilon$, $k-\omega$ and other turbulence closure schemes (e.g. Justesen, 1988; Fuhrman et al., 2009), large eddy simulation (LES, e.g. Salon et al., 2007) and direct numerical simulation (DNS, e.g. Spalart and Baldwin,

* Corresponding author.
E-mail address: d.a.vandera@abdn.ac.uk (D.A. van der A).

https://doi.org/10.1016/j.coastaleng.2022.104242
Received 1 August 2022; Received in revised form 21 September 2022; Accepted 25 October 2022
Available online 4 November 2022

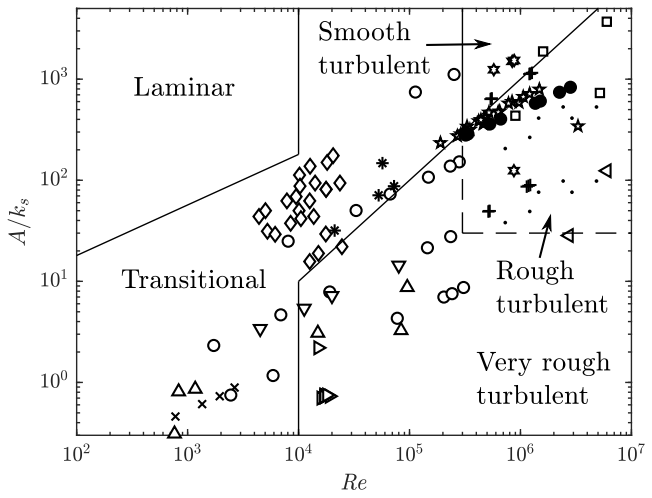

Fig. 1. Regime diagram showing previous studies of regular oscillatory flow over a rough wall. Markers denote Jonsson and Carlsen (1976, ◁), Kemp and Simons (1982, ×), Sleath (1987, ○), Jensen et al. (1989, □), Krstic and Fernando (2001, ◇), Mirfenderesk and Young (2003, △), Chen et al. (2007, ✱), Dixen et al. (2008, ▷), van der A et al. (2011, +), Yuan and Madsen (2014, ·), Ghodke and Apte (2016, ▽), Xie et al. (2021, ★), O'Donoghue et al. (2021, ✲), Dunbar (2022, ●). Delineation of flow regimes is based on Jonsson (1980) and Davies and Villaret (1997). Note that only the regular (i.e. non-modulated) flow cases of O'Donoghue et al. (2021) are included.

1987; Scandura et al., 2016; Ghodke and Apte, 2018; van der A et al., 2018) to simulate oscillatory boundary layer flow. While these modelling approaches offer considerable insight into the flow physics, they are generally too complex and computationally intensive to be used as practical engineering tools.

Some simpler models for oscillatory boundary layer flow have been proposed. Several authors have used the eddy viscosity hypothesis of Boussinesq (1877) as the basis for such a model. Taking this approach, the equation of motion in the boundary layer is given by

$$\frac{\partial}{\partial t}(u-u_\infty)=\frac{\partial}{\partial y}\left(\nu_t\frac{\partial u}{\partial y}\right) \tag{1}$$

where t is time, u is ensemble-averaged streamwise velocity, subscript $_\infty$ denotes a quantity in the free-stream, y is the vertical coordinate and ν_t is the eddy viscosity. Kajiura (1968), Grant and Madsen (1979), Brevik (1981) and Myrhaug (1982) proposed models where ν_t depends on y only and provided solutions for sinusoidal oscillatory flow. Trowbridge and Madsen (1984a,b), Davies (1986) and Gonzalez-Rodriguez and Madsen (2011) extended the work to ν_t that depends on both y and t for flows consisting of up to two harmonics in the free-stream. Yuan and Madsen (2015) developed a model that considered a larger number of flow harmonics. While the eddy viscosity approach gives useful results, fundamentally, these models have the weakness that they rely on assumed ν_t that are not always consistent with experimental data. Several authors (e.g. Jonsson and Carlsen, 1976; Sleath, 1987; Nielsen, 1985) pointed out that the shear stress and velocity gradient $\partial u/\partial y$ are generally not equal to zero at the same phase, leading to ν_t values that are negative or approach infinity at certain phases of the flow cycle (Nielsen, 1992). This behaviour leads to questions regarding the applicability of the eddy viscosity concept to oscillatory flows.

Another approach to modelling turbulent oscillatory boundary layers was developed by Nielsen (1985, 1992, 2016) and Teng et al. (2022). For the classical problem of laminar oscillatory flow over a smooth wall (e.g. Stokes, 1851), if the first harmonic of free-stream velocity is given by $u_{1,\infty}=\mathrm{Re}\left\{A_1\omega e^{i\omega t}\right\}$, where A_1 is the first harmonic orbital amplitude, the first harmonic velocity in the boundary layer is given by $u_1=\mathrm{Re}\left\{[1-D_1]A_1\omega e^{i\omega t}\right\}$, where the complex velocity defect $D_1=e^{-(1+i)y/\delta}$ and $\delta=\sqrt{2\nu/\omega}$ is the Stokes length. Nielsen (1985) noted that $\ln|D_1|=\arg(D_1)$ in this case and demonstrated that this identity also holds reasonably well for non-laminar experimental data from Kalkanis (1964), van Doorn (1981, 1982, 1983) and Sleath (1982), suggesting the general form of D_1 is Nielsen (1985, 2016)

$$D_1=\exp\left[-(1+i)\left(\frac{y}{\lambda_1}\right)^{p_1}\right] \tag{2}$$

where

$$p_1=0.59\exp\left[0.59\frac{1-\left(\frac{A_1}{38k_s}\right)^{1.8}}{1+\left(\frac{A_1}{38k_s}\right)^{1.8}}\right] \tag{3}$$

with universal vertical scale

$$\lambda_1=\sqrt{2\nu/\omega+0.0081k_sA_1}. \tag{4}$$

According to Nielsen (2016), this model holds when $Re<2.5\times10^4$ and $17<A/k_s<100$. When $Re>1.3\times10^5$ and $A/k_s>476$, $\ln|D_1|\neq\arg(D_1)$ but $|D_1|=e^{-(y/\lambda_1)^{p_1}}$ remains true, with $p_1=1/3$. It is worth noting that $\ln|D_1|=\arg(D_1)$ implies that the bottom phase lead of the first harmonic, ϕ_0, is equal to 45° (Nielsen, 1985). However, when $Re>1.3\times10^5$, ϕ_0 typically takes on values of 15°–30° (e.g. van der A et al., 2011; Yuan and Madsen, 2014) which may explain why $\ln|D_1|\neq\arg(D_1)$ in this range of Reynolds number.

Recently, Teng et al. (2022) proposed an improved version of the Nielsen (1985, 1992, 2016) model, applicable to a wider range of Re and A/k_s. They proposed a modified defect function that takes the form

$$D_1=\exp\left[-\left(\frac{y}{\lambda_1}\right)^{p_1}+i\left(\frac{y}{\lambda_2}\right)^{p_2}\right] \tag{5}$$

allowing flows for which $\ln|D_1|\neq\arg(D_1)$ to be modelled, and provided empirical expressions for λ_1, λ_2, p_1 and p_2 based on experimental and numerical data across a wide range of Re and A/k_s. Their model generally performed well across a range of flow regimes for approximation of the first harmonic of streamwise velocity, in some cases outperforming a far more computationally intensive $k-\omega$ turbulence model. However, the model of Teng et al. (2022) only predicts the first harmonic component of velocity. In practice, oscillatory flows under real waves have significant skewness and asymmetry, and multiple harmonic components are necessary to capture the flow shape.

This article presents a new practical model for the kinematics of oscillatory flow in the rough turbulent regime that is thoroughly validated against experimental data. The model is empirically based on experimental data from several previous studies and is applicable to flows comprised of multiple harmonic components. The article is organised as follows: Section 2 introduces the experimental datasets used for model calibration. The model is presented in Section 3. In Section 4, the model is validated using experimental data. Finally, Section 5 contains concluding remarks.

2. Experimental datasets

In this article, experimental data from several previous OFT experiments (Jonsson and Carlsen, 1976; van der A et al., 2011; Yuan and Madsen, 2014; O'Donoghue et al., 2021; Dunbar, 2022) are used to develop and validate the empirical model. In the experiments, velocity profiles in a periodic oscillatory boundary layer over a fixed rough bed were measured using particle image velocimetry (PIV), laser Doppler anemometry (LDA), or a micropropellor. The data cover a range of Re and A/k_s, primarily within the rough turbulent regime, and include flows that consist of multiple harmonic components. The data come from measurements made in 3 different OFT facilities. A summary of the flow conditions is presented in Table 1. Note that the values of A and Re reported in Table 1 may differ slightly to those given in the respective sources because of differences in the definitions used. k_s values in the table are the values reported in the respective sources. The

Table 1
Summary of flow conditions for experimental datasets. The superscripts after each flow identifier refer to the data source: 1-Jonsson and Carlsen (1976), 2-van der A et al. (2011), 3-Yuan and Madsen (2014), 4-O'Donoghue et al. (2021), 5-Dunbar (2022).

Flow identifier	Re ($\times 10^5$)	A/k_s	Sk_∞	As_∞
test no. 1[1]	53.4	116	−0.09	−0.04
test no. 2[1]	29.0	29	0.03	0.03
S505010c[2]	5.4	639	−0.04	0.08
S605010c[2]	5.5	641	−0.06	0.28
S755010c[2]	5.6	651	−0.06	0.61
S505010 g[2]	5.2	49	−0.01	0.08
S605010[2]g	5.3	50	−0.03	0.27
S755010 g[2]	5.3	50	−0.04	0.59
S507012c[2]	11.9	1119	−0.01	0.06
S607012c[2]	12.3	1136	0.01	0.26
S757012c[2]	13.1	1172	0.07	0.58
S507012 g[2]	11.4	86	−0.01	0.06
S607012 g[2]	11.9	88	0.01	0.26
S757012 g[2]	12.8	92	0.05	0.57
SP400a_sa[3]	33.9	445	0.00	−0.02
SP400b_sa[3]	16.2	435	−0.00	−0.02
SP250_sa[3]	13.1	277	0.01	−0.02
SP200_sa[3]	4.2	221	0.01	−0.01
ST400a_sa[3]	51.9	551	0.50	−0.06
ST400b_sa[3]	25.4	545	0.47	0.02
ST200_sa[3]	12.9	274	0.47	−0.06
FL320a_sa[3]	25.8	388	0.01	0.47
FL160_sa[3]	6.0	188	−0.01	0.48
SP400a_ce[3]	35.2	84	0.01	−0.03
SP400b_ce[3]	17.3	83	0.00	−0.03
SP250_ce[3]	13.9	53	0.00	−0.03
SP200_ce[3]	4.3	42	0.01	−0.02
ST400a_ce[3]	58.7	108	0.51	−0.11
ST200_ce[3]	15.2	55	0.50	−0.09
FL320a_ce[3]	28.6	76	−0.01	0.47
FL160_ce[3]	7.4	39	0.01	0.50
CSSR[4]	8.4	1500	−0.04	0.05
CSVR[4]	8.8	1531	0.42	0.10
CSAR[4]	5.8	1240	−0.02	0.42
GVVR[4]	8.7	124	0.42	0.11
SS0800[5]	3.2	280	−0.01	0.02
SK0800[5]	6.6	403	0.75	0.00
CB0800[5]	5.3	360	0.53	0.53
AS0800[5]	3.4	287	0.00	0.75
SS1549[5]	13.6	577	−0.02	0.01
SK1549[5]	28.2	831	0.75	0.01
CB1549[5]	22.5	742	0.51	0.53
AS1549[5]	15.1	607	0.03	0.76

data from each flow condition consist of ensemble-averaged velocity $u(y,t)$, with $y = 0$ corresponding to a representative roughness crest level (as defined in the respective sources), $0 \leq t < T$ and $t = 0$ corresponding to the phase of the zero-up crossing of $u_\infty = u(\max[y],t)$. Free-stream skewness Sk_∞ and asymmetry As_∞ are computed using

$$Sk = \overline{u_\mathrm{p}^3} \Big/ \left(\overline{u_\mathrm{p}^2}\right)^{\frac{3}{2}} \tag{6}$$

and

$$As = -\overline{[\mathcal{H}(u_\mathrm{p})]^3} \Big/ \left(\overline{u_\mathrm{p}^2}\right)^{\frac{3}{2}}, \tag{7}$$

respectively, where $u_\mathrm{p} = u - \overline{u}$ is the oscillating component of velocity, overbar denotes a time average and $\mathcal{H}$ is the Hilbert transform.

3. Model formulation

The present work considers the problem of oscillating flow driven by an unsteady periodic pressure gradient in the vicinity of a rough boundary. A one-dimensional ensemble-averaged flow field $u(y,t)$ is assumed. The flow described is practically identical to the flow inside an OFT. However, the steady streaming that normally occurs in an OFT is neglected. The magnitude of this streaming is typically <3% of $\max(u_\infty)$ (e.g. Yuan and Madsen, 2014). Hence, only the oscillating component of $u(y,t)$, $u_\mathrm{p}(y,t)$, is considered.

Using a Fourier decomposition, $u_\mathrm{p}(y,t)$ can be written

$$u_\mathrm{p}(y,t) = \sum_{n=1}^{N} \left[F_n(y)e^{in\omega t} + F_n^*(y)e^{-in\omega t}\right], \tag{8}$$

where F_n is the complex Fourier coefficient at frequency $n\omega$, * denotes complex conjugation and N is the number of harmonics that comprise the flow. Eq. (8) can be written in terms of real numbers as

$$u_\mathrm{p}(y,t) = \sum_{n=1}^{N} 2|F_n(y)|\cos(n\omega t + \arg[F_n(y)]). \tag{9}$$

Hence, the oscillating component of the free-stream velocity time-series with zero mean current can be written as

$$u_{\mathrm{p},\infty}(t) = \sum_{n=1}^{N} U_n \cos(n\omega t + \alpha_n) \tag{10}$$

where $U_n = 2|F_n(y \to \infty)|$ and $\alpha_n = \arg[F_n(y \to \infty)]$ are the amplitude and phase of the nth harmonic of free-stream velocity, respectively. Noting that the flow harmonics undergo an attenuation and phase shift within the boundary layer relative to the free-stream, the corresponding oscillatory velocity in the boundary layer can be written

$$u_\mathrm{p}(y,t) = \sum_{n=1}^{N} U_n K_n(y)\cos[n\omega t + \alpha_n + \phi_n(y)], \tag{11}$$

where

$$K_n(y) = 2|F_n(y)|/U_n \tag{12}$$

and

$$\phi_n(y) = \arg[F_n(y)] - \alpha_n \tag{13}$$

are the attenuation and phase lead of harmonic component n relative to the free-stream. In the classical smooth-wall laminar case, the exact analytical solutions for K_n and ϕ_n are (Svendsen, 2006)

$$K_n(y) = \sqrt{1 + e^{-2\sqrt{n}y/\delta} - 2e^{-\sqrt{n}y/\delta}\cos\left(\sqrt{n}y/\delta\right)} \tag{14}$$

and

$$\phi_n(y) = \tan^{-1}\left[\frac{e^{-\sqrt{n}y/\delta}\sin\left(\sqrt{n}y/\delta\right)}{1 - e^{-\sqrt{n}y/\delta}\cos\left(\sqrt{n}y/\delta\right)}\right], \tag{15}$$

respectively. In the case of rough turbulent flow, K_n and ϕ_n cannot be derived analytically due to the turbulence closure problem. Instead, empirical expressions for $K_n(y)$ and $\phi_n(y)$ can be extracted from experimental data. This approach is taken in the present work.

3.1. Assumption of frequency independence of K_n and ϕ_n

For discretely sampled data, the bispectrum of a time-series for frequency components ω_m and ω_n is given by (see Kim and Powers, 1979, for a derivation)

$$B(\omega_m,\omega_n) = \mathcal{E}(F_m F_n F_{m+n}^*), \tag{16}$$

where $\mathcal{E}$ denotes an ensemble average. Elgar and Guza (1985) and Elgar (1987) noted that for discretely sampled data, Sk and As are related to the real and imaginary parts of $B(\omega_m,\omega_n)$ by

$$Sk = \frac{12\sum_m\sum_n \mathrm{Re}[B(\omega_m,\omega_n)] + 6\sum_m^{N/2}\mathrm{Re}[B(\omega_m,\omega_m)]}{\left(\overline{u_\mathrm{p}^2}\right)^{\frac{3}{2}}} \tag{17}$$

and

$$As = -\frac{12\sum_m\sum_n \mathrm{Im}[B(\omega_m,\omega_n)] + 6\sum_m^{N/2}\mathrm{Im}[B(\omega_m,\omega_m)]}{\left(\overline{u_\mathrm{p}^2}\right)^{\frac{3}{2}}}, \tag{18}$$

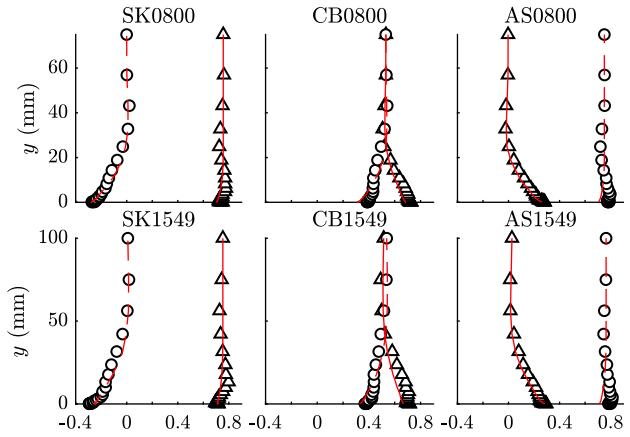

Fig. 2. Comparison of vertical profiles of Sk (triangles) and As (circles) with Eq. (20) (solid red line) and Eq. (21) (dashed red line) for non-sinusoidal flow cases of Dunbar (2022).

respectively, where $1 \leq m \leq N$, $1 \leq n \leq N$, $m > n$, $m + n \leq N$. By assuming each harmonic component of an oscillatory flow is subject to a frequency-independent attenuation K and phase shift ϕ within the boundary layer relative to the free-stream (i.e. $F_n = Ke^{i\phi}F_{n,\infty}$ for all n), the bispectrum within the boundary layer is given by

$$B(\omega_m, \omega_n) = \mathcal{E}(K^3 e^{i\phi} F_{m,\infty} F_{n,\infty} F^*_{m+n,\infty}). \tag{19}$$

Hence, the following equations for Sk and As can be derived following Henderson et al. (2004) and Berni et al. (2013):

$$Sk = \cos(\phi)Sk_\infty + \sin(\phi)As_\infty \tag{20}$$

$$As = \cos(\phi)As_\infty - \sin(\phi)Sk_\infty. \tag{21}$$

Numerical results from a RANS model (Henderson et al., 2004), as well as measurements from wave flume facilities (Berni et al., 2013; Henriquez et al., 2014; Fromant et al., 2018) have shown a relationship between Sk at a single vertical position, y, very close to the bed and Sk_∞ that agrees fairly well with Eq. (20) for transitional and turbulent flows, taking ϕ as the phase lead of the first flow harmonic as close to $y = 0$ as possible.

Fig. 2 compares vertical profiles of Sk and As from the non-sinusoidal experimental cases of Dunbar (2022) with Sk and As estimated using Eqs. (20) and (21), taking ϕ as $\phi_1(y)$ extracted from the experimental measurements. The figure shows that there is good agreement between the data and Eqs. (20) and (21) throughout the boundary layer, not just at $y \approx 0$. This suggests that the assumption of a frequency-independent K and ϕ allows for accurate estimation of the shape of the oscillatory velocity time-series throughout the boundary layer. This assumption is adopted for the present practical model, taking $K = K_1$ and $\phi = \phi_1$, to reduce the number of empirical expressions for K_n and ϕ_n necessary for closure of the model from N each to just one each. Hence, Eq. (11) is simplified to

$$u_p(y,t) = K_1(y) \sum_{n=1}^{N} U_n \cos[n\omega t + \alpha_n + \phi_1(y)]. \tag{22}$$

3.2. Empirical expressions for $K_1(y)$ and $\phi_1(y)$

Fig. 3 shows vertical profiles of K_1 and ϕ_1, obtained from all experimental flow cases in Table 1. Note that $K_1 \not\to 0$ as $y \to 0$. This is due to the definition that $y = 0$ corresponds to a representative roughness crest level, and there is some flow below this level. This definition is adopted because of its practicality, since for a known roughness topology, the vertical position of the theoretical bottom location obtained from a logarithmically fitted velocity profile is not known *a priori* and would require an additional empirical equation, whereas a suitably defined representative roughness crest level can be obtained directly from the known roughness topology. Fig. 4 shows vertical profiles of K_1 and ϕ_1/ϕ_0 where the vertical coordinate has been normalised by boundary layer thickness δ_{bl} as defined by Jensen et al. (1989), i.e. the y position at which $u = \max(u)$ at the phase when $u_\infty = \max(u_\infty)$. This definition of δ_{bl} has been shown to have a clear relationship with A/k_s of the form $\delta_{bl}/k_s = a\left(A/k_s\right)^b$, where a and b are empirical constants, by many previous authors (e.g. Jonsson, 1966; Fredsøe and Deigaard, 1992; van der A et al., 2011; Yuan and Madsen, 2014). The plots show that each set of profiles collapse reasonably well onto one line when this normalisation is applied. There is some variation in the plot of ϕ_1/ϕ_0. This is likely due to the uncertainty in determining the value of bottom phase lead, ϕ_0, because LDA and PIV measurements are less reliable in the vicinity of a boundary as a result of laser reflection, and the precise definition of $y = 0$ differs slightly between the respective experimental sources.

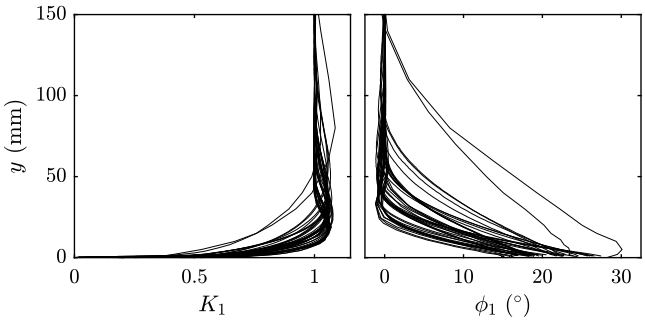

Fig. 3. Vertical profiles of K_1 and ϕ_1 from all experimental cases in Table 1.

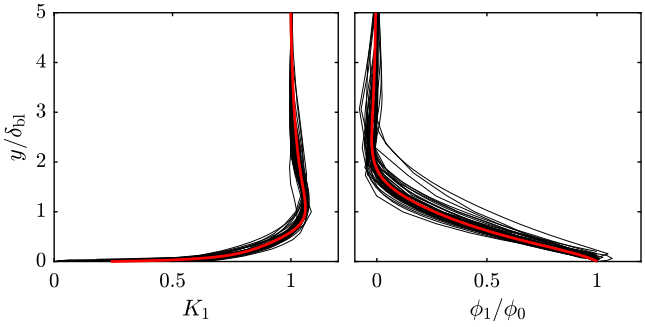

Fig. 4. Vertical profiles of K_1 and ϕ_1/ϕ_0 with the vertical coordinate normalised by δ_{bl} (black) and K_1 and ϕ_1/ϕ_0 given by Eqs. (23) and (24), respectively (red).

Also shown on each plot is a line fitted by least-squares regression to the mean of all the experimental profiles linearly interpolated onto an evenly spaced y array. Expressions for K_1 and ϕ_1 obtained from this fitting procedure are given by

$$K_1 = \begin{cases} \frac{0.98\hat{y}^3 - 0.77\hat{y}^2 + 0.57\hat{y} + 0.0079}{\hat{y}^3 - 0.87\hat{y}^2 + 0.58\hat{y} + 0.033} & \text{for} \quad \hat{y} \leq 5 \\ 1 & \text{for} \quad \hat{y} > 5 \end{cases} \tag{23}$$

and

$$\frac{\phi_1}{\phi_0} = \begin{cases} \frac{-0.70\hat{y} + 1.3}{\hat{y}^4 - 2.3\hat{y}^3 + 2.5\hat{y}^2 - 0.21\hat{y} + 1.3} & \text{for} \quad \hat{y} \leq 5 \\ 0 & \text{for} \quad \hat{y} > 5, \end{cases} \tag{24}$$

where $\hat{y} = y/\delta_{bl}$. It is assumed that $\hat{y} > 5$ is in the free-stream; hence $K_1 = 1$ and $\phi_1/\phi_0 = 0$ at $\hat{y} > 5$.

The boundary layer thickness δ_{bl} can be estimated using (van der A et al., 2011)

$$\frac{\delta_{bl}}{k_s} = 0.075\left(\frac{A_c}{k_s}\right)^{0.82}, \tag{25}$$

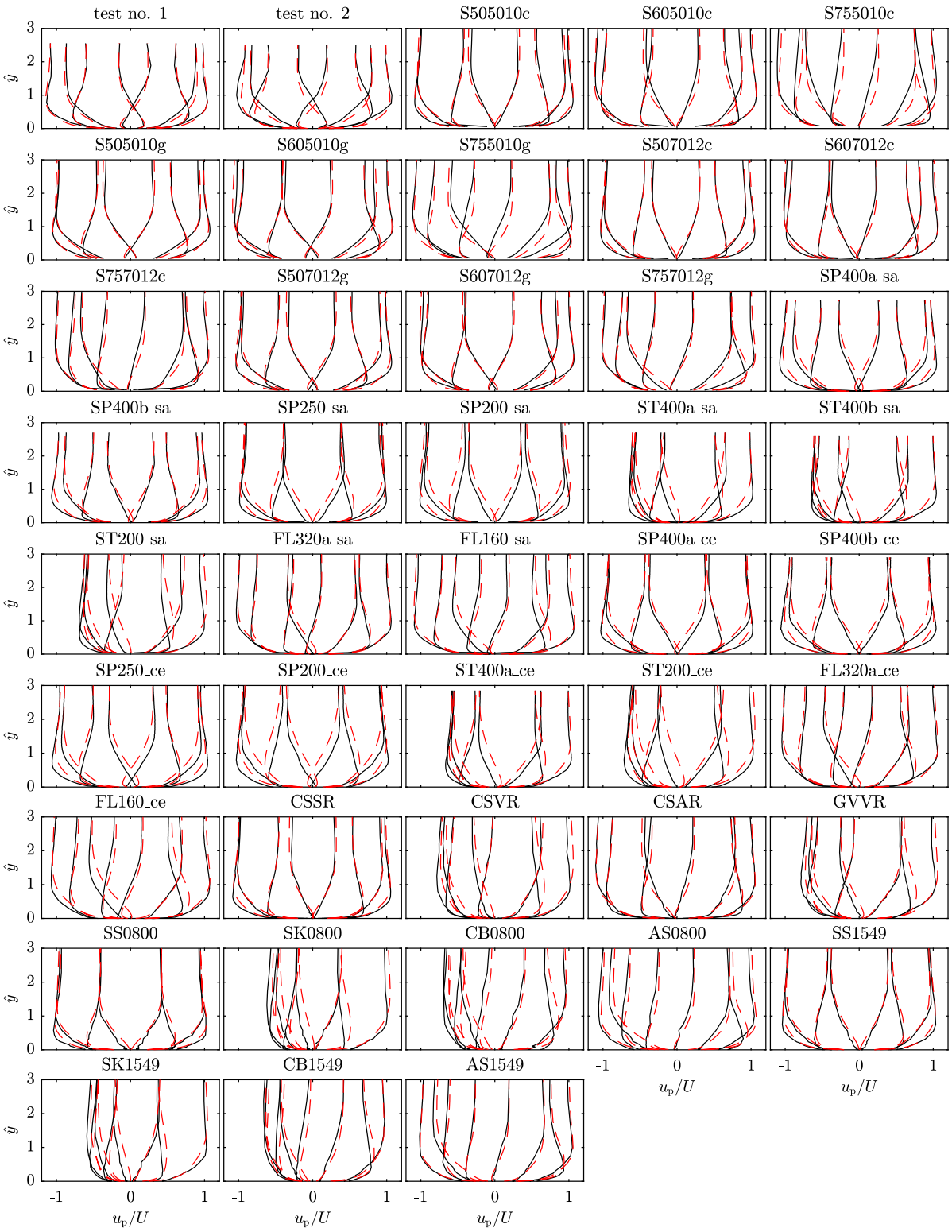

Fig. 5. Comparison of normalised vertical profiles of u_p from experimental data (solid black lines) and predicted by Eqs. (22)–(26) (dashed red lines) at 8 phases evenly distributed through the flow cycle for all flow conditions shown in Table 1. Both the experimental and predicted values of u_p are normalised by the experimental value of U and the vertical coordinates are normalised by δ_{bl} from experimental data.

where $A_c = 2AT_{ac}/T_c$ following Silva et al. (2006) and van der A et al. (2011), where T_c and T_{ac} are the times from the zero-up crossing of $u_\infty(t)$ to the zero-down crossing of $u_\infty(t)$ and the time that $u_\infty(t) = \max[u_\infty(t)]$, respectively.

The bottom phase lead ϕ_0 can be estimated using the expression of Humbyrd (2012), which for rough turbulent flow is as follows (ϕ_0 in degrees):

$$\phi_0 = \frac{180}{\pi}\left[0.649\left(\frac{A_1}{k_s}\right)^{-0.16} + 0.118\right]. \tag{26}$$

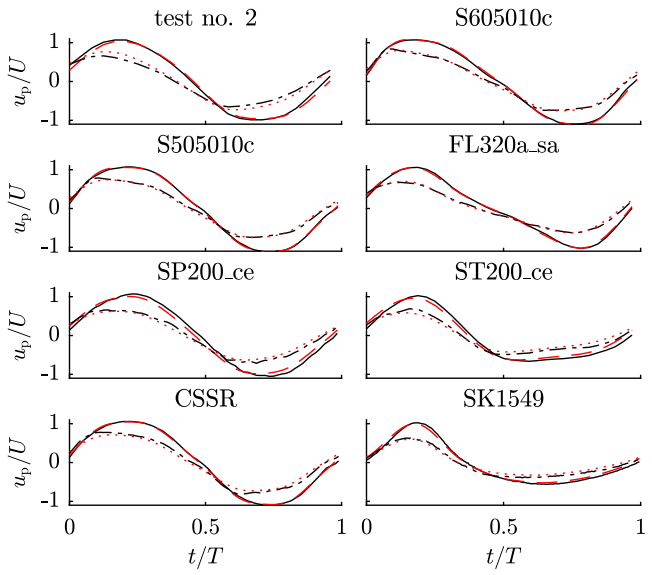

Fig. 6. Comparison of normalised time-series of u_p at $\hat{y} = 1$ (experimental: solid black line, predicted: dashed red line) and at the vertical position closest to $\hat{y} = 0.1$ (experimental: dash-dotted black line, predicted: dotted red line).

Eqs. (22)–(26) form a complete model for $u_p(y,t)$ in a rough turbulent oscillatory boundary layer for given k_s and u_∞. For flow over roughness with unknown k_s, k_s can be estimated using $k_s \approx 2d_{50}$, where d_{50} is median grain diameter, for roughness composed of fixed sand or gravel particles, or the expression of Flack et al. (2020),

$$k_s = \begin{cases} 2.73\sigma_y(2+sk_y)^{-0.45} & \text{for } sk_y < 0 \\ 2.11\sigma_y & \text{for } sk_y = 0 \\ 2.48\sigma_y(1+sk_y)^{2.24} & \text{for } sk_y > 0, \end{cases} \tag{27}$$

where σ_y and sk_y are the standard deviation and skewness of the roughness height field, respectively, can be used for roughness with known height field statistics.

4. Model validation

To test the performance of the model, a comparison of u_p from the experimental data shown in Table 1 is made with u_p computed using Eqs. (22)–(26). For each case shown in Table 1, input to the model is the measured u_∞ and the k_s reported by the authors for their respective experiments. For the comparison, N in Eq. (22) is set to 6. This value is excessive for the near-sinusoidal flows but is chosen to ensure that $u_{p,\infty}(t)$ is reproduced with sufficient accuracy for all flow cases.

Fig. 5 compares normalised vertical profiles of u_p interpolated onto 8 phases evenly distributed through the flow cycle. The figure shows that there is generally excellent agreement between the experimental data and the model, though in some cases a discrepancy can be observed. In all cases with significant Sk_∞, such as ST200_ce and SK1549, discrepancies between the experimental and predicted profiles are apparent. This may suggest that the assumption of a frequency-independent K and ϕ, which only becomes relevant for non-sinusoidal flows, could be a significant source of error in the model. However, the cases with significant As_∞ often exhibit very good agreement. For example, predicted and measured profiles in cases S605010c and FL320a_sa agree well despite As_∞ values of 0.28 and 0.47, respectively. It is worth noting that the experimental data used for model calibration contains more asymmetric than skewed flow cases, and most of the skewed flows have Sk_∞ values near 0.5, compared with the asymmetric flows that have more varied As_∞ values. Additionally, predicted profiles for some flows with near-zero values of Sk_∞ and As_∞, such as cases test no. 2 and SP200_ce, also deviate noticeably from the measured profiles despite not being affected by the assumption of frequency-independent K and ϕ. Hence, the assumption of frequency-independent K and ϕ is not necessarily a primary source of error in the model.

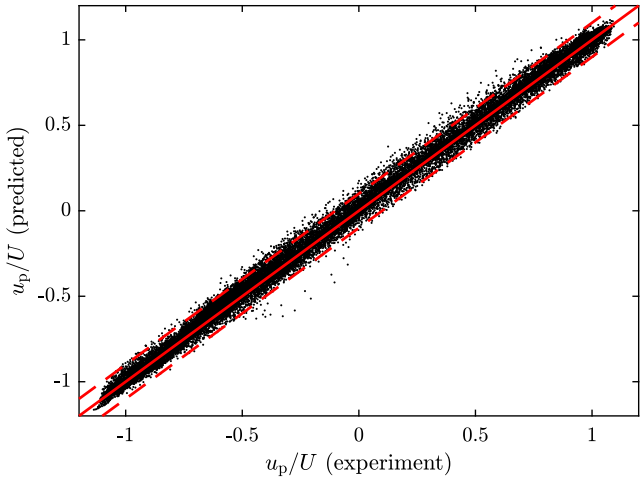

Fig. 7. Comparison of experimental and predicted $u_p(y',t')$ for all flow cases in Table 1 at all t' and y' (dots). Both axes are normalised by the experimental value of U. The solid and dashed red lines correspond to perfect agreement and $\pm 0.1U$ discrepancy, respectively.

Fig. 6 compares predicted and experimental normalised time-series of u_p at $\hat{y} = 1$ and at a vertical position from the respective experimental dataset as close to $\hat{y} = 0.1$ as possible for 8 selected flow cases. The left and right columns show the comparison for near-sinusoidal and significantly non-sinusoidal flows, respectively. The 8 selected cases include flows for which the agreement between experiment and model seen in Fig. 5 is very good (S505010c, CSSR, S605010c, FL320a_sa) and for which a clear discrepancy can be observed (test no. 2, SP200_ce, ST200_ce, SK1549). Even for cases for which discrepancies are visible, there is still good agreement between the predicted and experimental time-series.

To undertake a more quantitative assessment of the overall model performance across all flow cases shown in Table 1, experimental and predicted u_p values are compared. To ensure an equal number of comparisons are made for each flow case from Table 1, distributed evenly through the flow cycle and boundary layer, $u_p(y,t)$ is linearly interpolated onto new vertical and temporal coordinates, $0.05\delta_{bl} < y' \leq \min(\max[y], 5\delta_{bl})$, and $0 \leq t' < T$, with constant spacing, $\Delta y' = \min(\max[y], 5\delta_{bl})/25$ and $\Delta t' = T/32$, respectively. The lower limit of $y = 0.05\delta_{bl}$ is chosen to remove a small number of outliers that occur very close to $y = 0$ that result from slight differences in the definitions and methodology used to determine $y = 0$ between the respective experimental sources, and due to reduced LDA and PIV measurement accuracy in the vicinity of the bed; the upper limit of $y = 5\delta_{bl}$ is selected because above this level $K_1 = 1$ and $\phi_1 = 0$, so experimental and predicted values of u_p are identical if N is sufficiently large. Fig. 7 shows the comparison of measured and predicted $u_p(y',t')$ for all the flows in Table 1.

The figure shows that there is excellent overall agreement for these flow conditions, with nearly all predictions following the 1:1 line closely.

The normalised error between predicted and experimental kinematics can be computed using

$$\text{NE} = \frac{|u_p(\text{predicted}) - u_p(\text{experimental})|}{U}. \tag{28}$$

Fig. 8 shows the cumulative distribution function (CDF) of NE for all flow cases shown in Table 1 at all t' and y'. The figure demonstrates

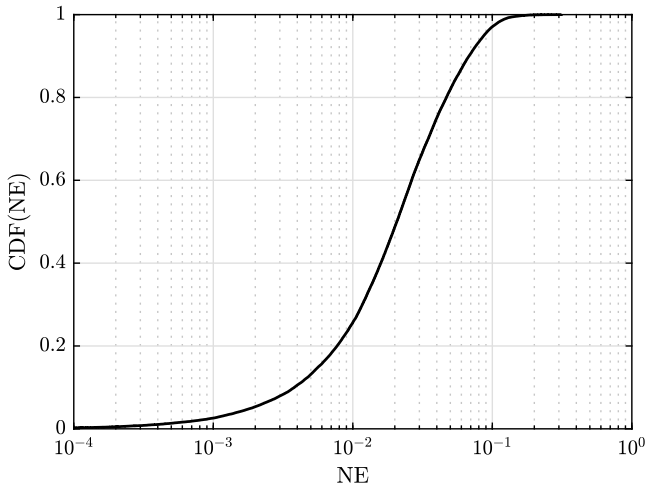

Fig. 8. CDF of NE from Eq. (28) for all data points shown in Fig. 7.

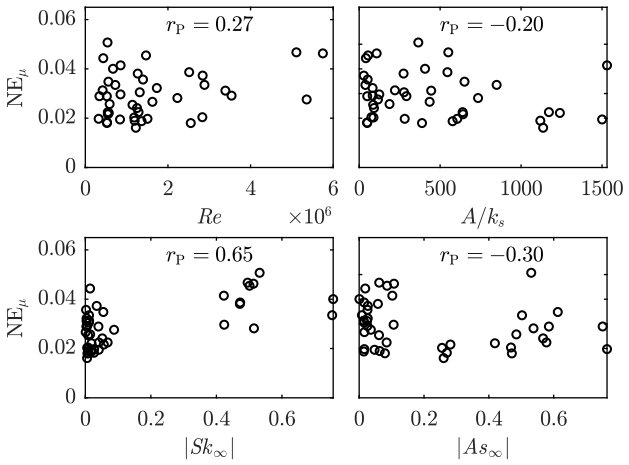

Fig. 9. Scatter plots of NE_μ versus Re (top-left), A/k_s (top-right), $|Sk_\infty|$ (bottom-left) and $|As_\infty|$ (bottom-right) for all flow cases shown in Table 1. Also shown are Pearson correlation coefficients r_P between NE_μ and the x-variable of each plot.

that 25%, 50% and 75% of the values of $u_p(y',t')$ have a normalised error of < 0.01, < 0.02 and < 0.04, respectively. Hence, the model performs very well overall in predicting u_p for a wide range of flow conditions primarily within the rough turbulent regime, throughout the boundary layer and flow cycle, with errors typically about two orders of magnitude smaller than U.

To obtain a more detailed insight into the model performance, the mean normalised error NE_μ is computed for each flow case using

$$\mathrm{NE}_\mu = \frac{1}{N_{y'}}\frac{1}{N_{t'}}\sum_{y'}\sum_{t'}\mathrm{NE}, \tag{29}$$

where $N_{y'}$ and $N_{t'}$ are the total number of y' and t' elements, respectively. Fig. 9 shows NE_μ plotted against Re, A/k_s, $|Sk_\infty|$ and $|As_\infty|$ to check if the performance is affected by any of these parameters. The Pearson correlation coefficients r_P between NE_μ and the x-variable of each plot are also shown. The data and r_P values show that there is no significant correlation between NE_μ and Re, A/k_s or $|As_\infty|$. Hence, changing these parameters within the range of the data used for model calibration does not affect the reliability of the model predictions. The value of $r_P = 0.65$ suggests that there may be a positive correlation between NE_μ and $|Sk_\infty|$. The most obvious reason for model prediction accuracy to be affected by $|Sk_\infty|$ is the error introduced by the assumption of a frequency-independent K and ϕ applied to all flow harmonics, since the influence of higher harmonics becomes important for flows with larger $|Sk_\infty|$. However, if this is the case, it would be expected that a correlation between NE_μ and $|As_\infty|$ would also exist, which is not seen in Fig. 9. Hence, it is plausible that the value $r_P = 0.65$ seen in the figure is not statistically significant, but results from the limited number of flows with significant $|Sk_\infty|$ used for validation, the majority of which have $|Sk_\infty|$ values very close to 0.5. A larger number of flows with significant $|Sk_\infty|$ taking on a more varied range of values would be necessary to determine with more certainty whether $|Sk_\infty|$ truly affects the reliability of model predictions.

5. Conclusions

A novel empirical model for the oscillating streamwise velocity in a rough turbulent oscillatory boundary layer has been presented. A summary of key features of the model is as follows.

The model is based around the assumption of a frequency-independent attenuation K_1 and phase lead ϕ_1 of each flow harmonic, an assumption that is demonstrated to be capable of accurately approximating the oscillating flow from experimental measurements. Empirical expressions for K_1 and ϕ_1 are extracted from experimental data from previous laboratory studies conducted in 3 distinct large-scale OFT facilities. The dataset covers 43 flow conditions, including flows comprised of multiple harmonic components. While the experimental data considered here are concentrated in the rough turbulent regime, in principle a similar empirical approach could be applied to experimental data from a range of flow regimes to obtain a more widely applicable model.

The model is simple to implement, requiring only the free-stream velocity time-series $u_\infty(t)$ and equivalent sand-grain roughness length k_s as inputs. Orbital amplitude A_c and flow frequency ω can be calculated from $u_\infty(t)$. Amplitudes and phases of the harmonic components of $u_\infty(t)$, U_n and α_n, and orbital amplitude A_1, can be obtained using the fast Fourier transform (FFT) algorithm. K_1, ϕ_1 and $u_p(y,t)$ can then be estimated by substitution into Eqs. (22)–(26).

The model has been shown to perform very well in predicting $u_p(y,t)$, with errors generally two orders of magnitude smaller than U. Additionally, the mean normalised error NE_μ of model predictions does not depend on Re, A/k_s or $|As_\infty|$. It is possible that flows with larger $|Sk_\infty|$ result in slightly reduced model accuracy, but further investigation is necessary to confirm if this is the case. Overall, the model is well-suited to engineering application due to its simplicity and accuracy.

The present model utilises data from OFT facilities to derive its empirical expressions. Since the flow in an OFT very closely approximates the bottom boundary layer under surface gravity waves, the model is likely to also allow accurate estimation of wave boundary layer kinematics; additionally, the small steady streaming that occurs in OFT facilities is neglected. The steady streaming under a surface gravity wave includes an additional contribution due to the streamwise inhomogeneity of the ensemble-averaged flow (e.g. Longuet-Higgins, 1953). The present model could, in principle, be linearly superposed with a model for the vertical profile of steady streaming to form a complete model for the ensemble-averaged flow in a rough turbulent oscillatory boundary layer under surface gravity waves. More experimental data are needed to test and develop the model for application to combined wave–current flow.

The new model is well-suited to forming the basis for an improved sediment transport model for rough turbulent oscillatory flow, since it offers practical predictions for the kinematics within the boundary layer which are generally not considered in existing sediment transport models. For this purpose, a prediction of intra-period bed shear stress, $\tau_0(t)$, which is not included in the present model, would also be necessary. An engineering predictor for $\tau_0(t)$ in an oscillatory boundary layer such as that proposed by Larsen and Fuhrman (2019), which does not require

any additional *a priori* knowledge to be implemented, could be used in conjunction with the present model to allow prediction of both $u_p(y,t)$ and $\tau_0(t)$ for the purpose of sediment transport model development.

CRediT authorship contribution statement

Danny Dunbar: Conceptualization, Methodology, Formal analysis, Investigation, Writing – original draft, Writing – review & editing, Visualization, Project administration, Funding acquisition. **Dominic A. van der A:** Conceptualization, Methodology, Resources, Writing – review & editing, Supervision, Funding acquisition. **Tom O'Donoghue:** Conceptualization, Methodology, Resources, Writing – review & editing, Supervision, Funding acquisition. **Pietro Scandura:** Conceptualization, Methodology, Resources, Writing – review & editing, Supervision, Funding acquisition.

Declaration of competing interest

The authors declare that they have no known competing financial interests or personal relationships that could have appeared to influence the work reported in this paper.

Data availability

Data will be made available on request.

Acknowledgements

This work was conducted as part of the first author's Ph.D., funded by The Carnegie Trust for the Universities of Scotland (grant no. PHD007716), and is also included in Dunbar (2022). The authors are grateful to Dr. Jing Yuan (Tsinghua University) for providing the experimental data from Yuan and Madsen (2014).

References

Berni, C., Barthélemy, E., Michallet, H., 2013. Surf zone cross-shore boundary layer velocity asymmetry and skewness: An experimental study on a mobile bed. J. Geophys. Res.: Oceans 118 (4), 2188–2200. http://dx.doi.org/10.1002/jgrc.20125.

Boussinesq, J., 1877. Essai sur la théorie des eaux courantes. Mémoires Présentés Par Divers Savants À L'Académie Des Sciences 23 (1), 1–64.

Brevik, I., 1981. Oscillatory rough turbulent boundary layers. J. Waterw. Port Coast. Ocean Div. 107 (3), 175–188. http://dx.doi.org/10.1061/JWPCDX.0000261.

Chen, D., Chen, C., Tang, F.E., Stansby, P., Li, M., 2007. Boundary layer structure of oscillatory open-channel shallow flows over smooth and rough beds. Exp. Fluids 42, 719–736. http://dx.doi.org/10.1007/s00348-007-0280-8.

Davies, A., 1986. A model of oscillatory rough turbulent boundary layer flow. Estuar. Coast. Shelf Sci. 23, 353–374. http://dx.doi.org/10.1016/0272-7714(86)90033-8.

Davies, A.G., Villaret, C., 1997. Oscillatory Flow over Rippled Beds: Boundary Layer Structure and Wave-Induced Eulerian Drift. In: Gravity Waves in Water of Finite Depth. Computational Mechanics Publications, Southampton, pp. 215–254.

Dibajnia, M., Watanabe, A., 1998. Transport rate under irregular sheet flow conditions. Coast. Eng. 35 (3), 167–183. http://dx.doi.org/10.1016/S0378-3839(98)00034-9.

Dixen, M., Hatipoglu, F., Sumer, B.M., Fredsøe, J., 2008. Wave boundary layer over a stone-covered bed. Coast. Eng. 55, 1–20. http://dx.doi.org/10.1016/j.coastaleng.2007.06.005.

Dunbar, D., 2022. Turbulent oscillatory flow over an irregular rough wall (Ph.D. thesis). University of Aberdeen, p. 182.

Elgar, S., 1987. Relationships involving third moments and bispectra of a harmonic process. IEEE Trans. Acoust. Speech Signal Process. 35 (12), 1725–1726. http://dx.doi.org/10.1109/TASSP.1987.1165090.

Elgar, S., Guza, R.T., 1985. Observations of bispectra of shoaling surface gravity waves. J. Fluid Mech. 161, 425. http://dx.doi.org/10.1017/S0022112085003007.

Flack, K.A., Schultz, M.P., Barros, J.M., 2020. Skin friction measurements of systematically-varied roughness: Probing the role of roughness amplitude and skewness. Flow Turbul. Combust. 104 (2–3), 317–329. http://dx.doi.org/10.1007/s10494-019-00077-1.

Fredsøe, J., Deigaard, R., 1992. Mechanics of Coastal Sediment Transport. World Scientific, Singapore, http://dx.doi.org/10.1142/1546.

Fromant, G., Hurther, D., van der Zanden, J., van der A, D.A., Cáceres, I., O'Donoghue, T., Ribberink, J.S., 2018. Wave boundary layer hydrodynamics and sheet flow properties under large-scale plunging-type breaking waves. J. Geophys. Res.: Oceans http://dx.doi.org/10.1029/2018JC014406, 2018JC014406.

Fuhrman, D.R., Fredsøe, J., Sumer, B.M., 2009. Bed slope effects on turbulent wave boundary layers: 2. Comparison with skewness, asymmetry, and other effects. J. Geophys. Res. 114 (C3), C03025. http://dx.doi.org/10.1029/2008JC005053.

Ghodke, C.D., Apte, S.V., 2016. DNS study of particle-bed-turbulence interactions in an oscillatory wall-bounded flow. J. Fluid Mech. 792, 232–251. http://dx.doi.org/10.1017/jfm.2016.85.

Ghodke, C.D., Apte, S.V., 2018. Roughness effects on the second-order turbulence statistics in oscillatory flows. Comput. & Fluids 162, 160–170. http://dx.doi.org/10.1016/j.compfluid.2017.09.021.

Gonzalez-Rodriguez, D., Madsen, O.S., 2011. Boundary-layer hydrodynamics and bed-load sediment transport in oscillating water tunnels. J. Fluid Mech. 667, 48–84. http://dx.doi.org/10.1017/S0022112010004337.

Grant, W.D., Madsen, O.S., 1979. Combined wave and current interaction with a rough bottom. J. Geophys. Res.: Oceans 84 (C4), 1797–1808. http://dx.doi.org/10.1029/JC084iC04p01797.

Henderson, S.M., Allen, J.S., Newberger, P.A., 2004. Nearshore sandbar migration predicted by an eddy-diffusive boundary layer model. J. Geophys. Res. C: Oceans 109 (6), C06024. http://dx.doi.org/10.1029/2003JC002137.

Henriquez, M., Reniers, A.J.H.M., Ruessink, B.G., Stive, M.J.F., 2014. PIV measurements of the bottom boundary layer under nonlinear surface waves. Coast. Eng. 94, 33–46. http://dx.doi.org/10.1016/j.coastaleng.2014.08.004.

Humbyrd, C.J., 2012. Turbulent Combined Wave-Current Boundary Layer Model for Application in Coastal Waters (Ph.D. thesis). Massachusetts Institute of Technology, p. 157.

Jensen, B.L., Sumer, B.M., Fredsøe, J., 1989. Turbulent oscillatory boundary layers at high Reynolds numbers. J. Fluid Mech. 206, 265–297. http://dx.doi.org/10.1017/S0022112089002302.

Jonsson, I.G., 1966. Wave boundary layers and friction factors. In: Coastal Engineering. American Society of Civil Engineers, New York, NY, pp. 127–148. http://dx.doi.org/10.1061/9780872620087.010.

Jonsson, I.G., 1980. A new approach to oscillatory rough turbulent boundary layers. Ocean Eng. 7 (1), 109–152. http://dx.doi.org/10.1016/0029-8018(80)90034-7.

Jonsson, I.G., Carlsen, N.A., 1976. Experimental and theoretical investigations in an oscillatory turbulent boundary layer. J. Hydraul. Res. 14 (1), 45–60. http://dx.doi.org/10.1080/00221687609499687.

Justesen, P., 1988. Prediction of turbulent oscillatory flow over rough beds. Coast. Eng. 12, 257–284. http://dx.doi.org/10.1016/0378-3839(88)90008-7.

Kajiura, K., 1968. A model of the bottom boundary layer in water waves. Bull. Earthquake Res. Inst. Univ. Tokyo 46, 75–123.

Kalkanis, G., 1964. Transportation of bed material due to wave action. Technical Report, U.S. Army Coastal Engineering Research Center.

Kemp, P.H., Simons, R.R., 1982. The interaction between waves and a turbulent current: waves propagating with the current. J. Fluid Mech. 116, 227–250. http://dx.doi.org/10.1017/S0022112082000445.

Kim, Y.C., Powers, E.J., 1979. Digital Bispectral Analysis and Its Applications to Nonlinear Wave Interactions. IEEE Trans. Plasma Sci. 7 (2), 120–131. http://dx.doi.org/10.1109/TPS.1979.4317207.

King, D., 1991. Studies in Oscillatory Flow Bedload Sediment Transport (Ph.D. thesis). UC San Diego, pp. 1–183.

Krstic, R.V., Fernando, H.J.S., 2001. The nature of rough-wall oscillatory boundary layers. J. Hydraul. Res. 39, 655–666. http://dx.doi.org/10.1080/00221686.2001.9628294.

Larsen, B.E., Fuhrman, D.R., 2019. Full-scale CFD simulation of tsunamis. Part 2: Boundary layers and bed shear stresses. Coast. Eng. 151, 42–57. http://dx.doi.org/10.1016/j.coastaleng.2019.04.011.

Longuet-Higgins, M.S., 1953. Mass transport in water waves. Phil. Trans. R. Soc. A 245 (903), 535–581. http://dx.doi.org/10.1098/rsta.1953.0006.

Malarkey, J., Davies, A.G., 2012. Free-stream velocity descriptions under waves with skewness and asymmetry. Coast. Eng. 68, 78–95. http://dx.doi.org/10.1016/j.coastaleng.2012.04.009.

Mirfenderesk, H., Young, I.R., 2003. Direct measurements of the bottom friction factor beneath surface gravity waves. Appl. Ocean Res. 25, 269–287. http://dx.doi.org/10.1016/j.apor.2004.02.002.

Myrhaug, D., 1982. On a theoretical model of rough turbulent wave boundary layers. Ocean Eng. 9, 547–565. http://dx.doi.org/10.1016/0029-8018(82)90002-6.

Nielsen, P., 1985. On the structure of oscillatory boundary layers. Coast. Eng. 9 (3), 261–276. http://dx.doi.org/10.1016/0378-3839(85)90011-0.

Nielsen, P., 1992. Coastal Bottom Boundary Layers and Sediment Transport. World Scientific, Singapore, http://dx.doi.org/10.1142/1269.

Nielsen, P., 2016. 1DV structure of turbulent wave boundary layers. Coast. Eng. 112, 1–8. http://dx.doi.org/10.1016/j.coastaleng.2016.02.001.

Nikuradse, J., 1933. Strömungsgesetze in rauhen rohren [laws of flow in rough pipes]. VDI Forschungsheft 361.

O'Donoghue, T., Davies, A.G., Bhawanin, M., van der A, D.A., 2021. Measurement and prediction of bottom boundary layer hydrodynamics under modulated oscillatory flows. Coast. Eng. 103954. http://dx.doi.org/10.1016/j.coastaleng.2021.103954.

Salon, S., Armenio, V., Crise, A., 2007. A numerical investigation of the Stokes boundary layer in the turbulent regime. J. Fluid Mech. 570, 253. http://dx.doi.org/10.1017/S0022112006003053.

Scandura, P., Faraci, C., Foti, E., 2016. A numerical investigation of acceleration-skewed oscillatory flows. J. Fluid Mech. 808, 576–613. http://dx.doi.org/10.1017/jfm.2016.641.

Silva, P.A., Abreu, T., van der A, D.A., Sancho, F., Ruessink, B.G., van der Werf, J., Ribberink, J.S., 2011. Sediment transport in nonlinear skewed oscillatory flows: Transkew experiments. J. Hydraul. Res. 49 (SUPPL.1), 72–80. http://dx.doi.org/10.1080/00221686.2011.592681.

Silva, P.A., Temperville, A., Seabra Santos, F., 2006. Sand transport under combined current and wave conditions: A semi-unsteady, practical model. Coast. Eng. 53 (11), 897–913. http://dx.doi.org/10.1016/j.coastaleng.2006.06.010.

Sleath, J.F.A., 1982. The effect of jet formation on the velocity distribution in oscillatory flow over flat beds of sand or gravel. Coast. Eng. 6 (2), 151–177. http://dx.doi.org/10.1016/0378-3839(82)90003-5.

Sleath, J.F.A., 1987. Turbulent oscillatory flow over rough beds. J. Fluid Mech. 182, 369–409. http://dx.doi.org/10.1017/S0022112087002374.

Spalart, P.R., Baldwin, B.S., 1987. Direct simulation of a turbulent oscillating boundary layer. In: 6th Symposium on Turbulent Shear Flows. Toulouse, pp. 417–440.

Stokes, G.G., 1851. On the effect of the internal friction of fluids on the motion of pendulums. In: Mathematical and Physical Papers. Cambridge University Press, Cambridge, pp. 1–10. http://dx.doi.org/10.1017/CBO9780511702266.002.

Svendsen, I.A., 2006. Introduction to Nearshore Hydrodynamics. World Scientific, Singapore, http://dx.doi.org/10.1142/5740.

Teng, Y., Lu, L., Cheng, L., Tong, F., Tang, G., 2022. A modified defect function for wave boundary layers. Coast. Eng. 171 (February 2021), 104050. http://dx.doi.org/10.1016/j.coastaleng.2021.104050.

Trowbridge, J., Madsen, O.S., 1984a. Turbulent wave boundary layers: 1. Model formulation and first-order solution. J. Geophys. Res. 89, 7989. http://dx.doi.org/10.1029/JC089iC05p07989.

Trowbridge, J., Madsen, O.S., 1984b. Turbulent wave boundary layers: 2. Second-order theory and mass transport. J. Geophys. Res. 89, 7999. http://dx.doi.org/10.1029/JC089iC05p07999.

van der A, D.A., O'Donoghue, T., Davies, A.G., Ribberink, J.S., 2011. Experimental study of the turbulent boundary layer in acceleration-skewed oscillatory flow. J. Fluid Mech. 684, 251–283. http://dx.doi.org/10.1017/jfm.2011.300.

van der A, D.A., O'Donoghue, T., Ribberink, J.S., 2010. Measurements of sheet flow transport in acceleration-skewed oscillatory flow and comparison with practical formulations. Coast. Eng. 57 (3), 331–342. http://dx.doi.org/10.1016/j.coastaleng.2009.11.006.

van der A, D.A., Scandura, P., O'Donoghue, T., 2018. Turbulence statistics in smooth wall oscillatory boundary layer flow. J. Fluid Mech. 849, 192–230. http://dx.doi.org/10.1017/jfm.2018.403.

van Doorn, T., 1981. Experimental investigation of near-bottom velocities in water waves without and with a current. Technical Report, Delft Hydraulics Laboratory.

van Doorn, T., 1982. Experimenteel onderzoek naar het snelheidsveld in de turbulente bodemgrenslaag in een oscillerende stroming in een golftunnel: rapport van metingen en gegevensverwerking. Technical Report, Delft Hydraulics Laboratory.

van Doorn, T., 1983. Computations and comparison with measurements of the turbulent bottom boundary layer in an oscillatory flow. Technical Report, Delft Hydraulics Laboratory.

Xie, M., Zhang, C., Li, J., Li, S., Yang, Z., Zhang, H., Qu, K., 2021. Flow structure and bottom friction of the nonlinear turbulent boundary layer under stormy waves. Coast. Eng. 164, http://dx.doi.org/10.1016/j.coastaleng.2020.103811.

Yuan, J., Madsen, O.S., 2014. Experimental study of turbulent oscillatory boundary layers in an oscillating water tunnel. Coast. Eng. 89, 63–84. http://dx.doi.org/10.1016/j.coastaleng.2014.03.007.

Yuan, J., Madsen, O.S., 2015. Experimental and theoretical study of wave-current turbulent boundary layers. J. Fluid Mech. 765, 480–523. http://dx.doi.org/10.1017/jfm.2014.746.